

Electrical Conductivity Constraints on the Geometry of the Western LATEA Boundary from a Magnetotelluric Data Acquired Near Tahalgha Volcanic District (Hoggar, Southern Algeria)



A. Bouzid, A. Bendekken, A. Deramchi, A. Abtout, N. Akacem, M. Djeddi and M. Hamoudi

Abstract The lithospheric structure of the Hoggar massif remains relatively unknown. The lack of high-resolution geophysical studies devoted to it is the source of controversial debates about its underlying structure and its geodynamics. This study targets the western edge of the LATEA microcontinent at the intersection of the 4°50′ sub-meridian major fault and the 4°35′ fault with the oued Ameded NE–SW lineament. The study area also includes the northern flank of the Tahalgha Cenozoic Volcanic District. The analysis and modeling of magnetotelluric data collected at 12 sites forming an EW profile of 75 km length made it possible to build a resistivity model over a hundred km of depth. The magnetotelluric data reveal a heterogeneous upper crust made up of probably very compact and

A. Bouzid (✉) · A. Deramchi · A. Abtout
Division Géophysique de Subsurface, CRAAG, BP 63,
Route de l’Observatoire, Algiers 16340, Algeria
e-mail: a.bouzid@craag.dz

A. Deramchi
e-mail: aboubakarderamchi@gmail.com

A. Abtout
e-mail: a.abtout@craag.dz

A. Bendekken · N. Akacem
Unité de Recherche de Tamanrasset, CRAAG, BP 32,
Tamanrasset 11000, Algeria
e-mail: a_bendekken@yahoo.fr

N. Akacem
e-mail: akacemn@yahoo.com

A. Deramchi · M. Djeddi · M. Hamoudi
Département de Géophysique, FSTGAT, USTHB, BP 32,
Al Alia, Dar el Beida, Algiers 16123, Algeria
e-mail: dallidjeddi@gmail.com

M. Hamoudi
e-mail: hamoudi@ipgp.fr

mechanically strong, electrically resistive structures corresponding to hypovolcanic granitoid and batholiths, and others more conductive probably more inhomogeneous, weak and more fractured corresponding to the Paleoproterozoic metamorphic basement. On the contrary, the lower crust and the lithospheric mantle down to a depth of about 100 km are fairly homogeneous. The 4°50' mega-fault is rooted into the lithospheric mantle to a depth of about 70 km. This is corroborated by potential field data to at least the base of the crust. By comparison, the 4°35' fault does not appear as important. The fault network highlighted by the magnetotelluric data has probably been used to transport melt from the asthenosphere up to the surface to give rise to the Tahalgha volcanic district. The fluids released or the precipitated mineralization are at the origin of the strong fall of the resistivity which gives a signature so peculiar to these faults.

Keywords Hoggar · LATEA · Tahalgha volcanic district · 4°50' fault
Magnetotellurics

1 Introduction

The present study focuses on a geologically complex area located on the western edge of LATEA at the intersection of the major sub-meridian 4°50' mega-fault with the NE–SW to ENE–WSW oued Ameded lineament and the location of the Tahalgha volcanic district. Indeed, the geological structure underlying this area has been shaped by the different major geological events that have affected the African plate since the Precambrian. According to Liégeois et al. (2003), it corresponds to the closure during the Neoproterozoic of an oceanic domain followed by the accretion of island arcs against the LATEA microcontinent. This old suture zone appears today at the surface to be the sub-meridian 4°50' mega-fault. In Pan-African times, during the formation of Gondwana, an intracontinental oblique convergence between the West African Craton and the Saharan Metacraton shaped the current structure of the Tuareg Shield and caused the dislocation of LATEA and the reactivation of the 4°50' fault. This shear zone allowed a displacement of several hundreds of km on both sides. The opening of the South Atlantic had induced distensive movements within the African continent and the creation of numerous aborted rifts among which that located along the lineament of oued Ameded. In the field, this lineament is represented by a corridor along which a large concentration of NE–SW faulting can be noticed. The magmatic districts of Tahalgha, Atakot/Manzaz, and Adrar N'Ajjer are also aligned along this lineament (Dautria and Lesquer 1989; Aït-Hamou and Dautria 1994). During the Cenozoic, the convergence between African and Eurasian plates resulted in a remote reactivation of the Tuareg shear zones and the advent of a tholeiitic volcanism in the center of the LATEA and alkaline volcanism towards the edges (Liégeois et al. 2005 and references therein). The volcanic district of Tahalgha is located at the periphery of

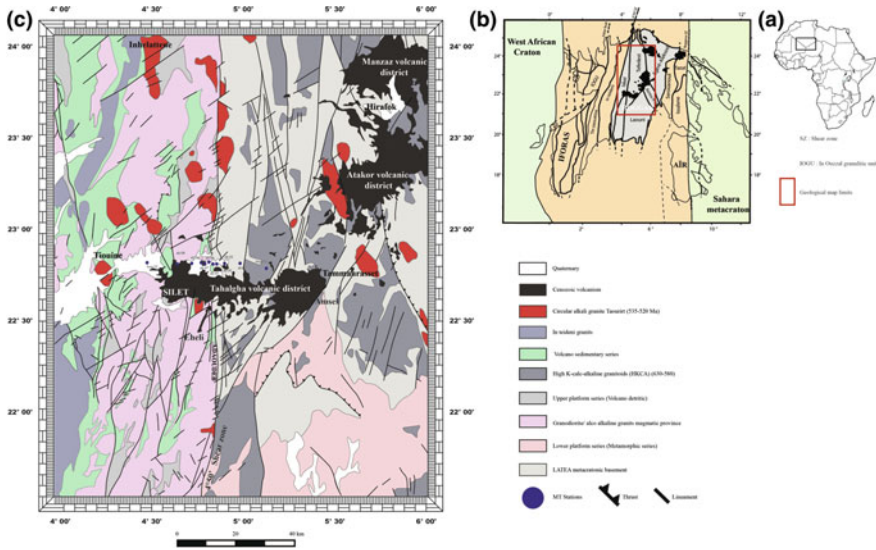


Fig. 1 The location of the Tuareg shield on the African continent map (in **a**), the location of the study region on a schematic map of the Tuareg shield (in **b**, after Black et al. 1994; Liégeois et al. 2003), and a simplified geological map of the study area (modified from Bertrand and Caby 1977; Zerrouk et al. 2016; in **c**)

LATEA, at the intersection of the fault 4°50' and the lineament of oued Ameded. It showed intense volcanic activity during the Neogene and the Quaternary (Fig. 1).

The Hoggar Shield has been well studied from surface geology, petrology, and xenoliths (Liégeois et al. 2003 and references therein; Dautria et al. 1988; Kourim et al. 2014). However, its deep structure (crustal and lithospheric) remains relatively unknown due to the paucity of geophysical studies (e.g., Bouzid et al. 2015). This is at the origin of controversies about its deep structure and its geodynamics. Global or continent-wide geophysical studies do not adequately resolve its underlying lithospheric structure, particularly beneath the volcanic districts and the mega-shear zones (Crough 1981; Lesquer et al. 1988; Pasyanos and Walter 2002; Sebäi et al. 2006; Gangopadhyay et al. 2007; Fishwick and Bastow 2011; Rougier et al. 2013). High-resolution geophysical studies are therefore of great importance in constraining the underlying geological structure of this region, thus bringing some elements into the debate on its deep structure.

Magnetotelluric (MT) is a passive geophysical method able to probe the crustal and upper mantle geological structure. From surface measurements of the natural telluric currents and the terrestrial magnetic field rapid fluctuations, the MT method allows to infer the distribution of the electrical conductivity in the lithosphere. Indeed, for a stratified Earth, and for a given frequency, the electrical resistivity of the lithosphere is proportional to the square of the ratio of the electric field component to the magnetic field perpendicular component (Tikhonov 1950; Cagniard 1953). The penetration depth of the electromagnetic energy is proportional to the

square root of the duration of the recordings. For broadband measurements and for an old and resistive crust like that of the Hoggar massif, this depth can reach a hundred km or more. The adoption of a suitable measurement step between stations and an optimal duration of the measurements in each of the stations, enables to image with an adapted resolution the lithospheric electrical conductivity distribution under the studied region.

The bulk electrical conductivity (inverse of resistivity) of a rock can be an excellent geological marker. Indeed, the conductivity is poorly correlated with the nature of the rock matrix but highly controlled with the porosity, the presence of fluids, mineralization or melt as well as with the thermodynamic conditions that prevail in the crust and in the upper mantle. In the crust as a whole, the increase in pressure with depth reduces substantially the volume of pores and thus causes a strong increase in the resistivity of rocks. In the lower crust, however, the presence of fluids or graphite induces a significant drop in resistivity. The resistivity increases moderately in the lithospheric mantle (Haak 1980; Lastoviskova 1983; Shankland and Ander 1983; Jödicke 1992; Jones 1999; Jones and Ferguson 2001; Nover 2005; Jones 2013).

Furthermore, the lithospheric electrical resistivity may vary laterally for several reasons. Old suture zones may be areas of strong falls in resistivity due to sediments trapped during ocean closure or due to the presence of volcanic rocks formed during the collision (Gokarn et al. 2002; Rao et al. 2007, 2014). Similarly, the existence of faults and shear zones in the lithosphere which can act as drain for the circulation of fluids or zones of mineralization precipitation, or even zones of weakness allowing magma rising to the surface, are generally associated with a sharp drop in resistivity (see for example Jones et al. 1992; Ritter et al. 2003; Unsworth and Bedrosian 2004; Bouzid et al. 2008, 2015). The rise of melt through the lithospheric faults and their spreading under the Moho or under the upper crust, as well as the existence of crustal volcanic chambers and reservoirs, may also induce sharp falls in the electrical resistivity within the lithosphere (Wannamaker et al. 2008; Meqbel et al. 2014; Bouzid et al. 2015).

In the present study, magnetotelluric broadband data collected at 12 sites in the Silet/Abalessa area of the Hoggar region will be analyzed and modeled. A 2D lithospheric resistivity model will be proposed and will be interpreted in geological terms.

2 Geological and Geophysical Settings

The Tuareg Shield, situated in North Western Africa, is composed of three massifs, the Hoggar in Algeria, the Adrar des Iforas in Mali and the Air in Niger. Important sub-meridian lithospheric shear zones ($4^{\circ}50'$ and $8^{\circ}30'$) characterize the structuration of the Hoggar as dislocated blocks (Caby 2003). Historically, this led to subdivide it into three parts, the Western Hoggar, the Central Polycyclic Hoggar and the Eastern Hoggar (Fig. 1). Later, the Tuareg Shield has been shown to be

composed of 23 terranes (Black et al. 1994) that mostly are superposed on the previous subdivision. Especially, the terranes composing most of the Central Polycyclic Hoggar (Laouni, Azrou-n-fad, Tefedest, Egéré-Aleksod) have been shown to have a common history and have been grouped within the LATEA (acronym of the above terranes) metacraton (Liégeois et al. 2003), an Archeo-Eburnean basement partially reactivated during the Pan-African orogeny. The metacraton LATEA (Liégeois et al. 2003) had a complex history, it has been affected by an Eburnean highgrade metamorphism (amphibolite- to granulite-facies 2.1-1.9 Ga; Bendaoud et al. 2008). After that, LATEA has been dissected by shear zones along which high-K calc-alkaline granitoid batholiths has been implemented, generating local high-temperature amphibolite facies metamorphism (Bendaoud et al. 2008). During the Mesoproterozoic, LATEA was cratonized by acquiring a rigid lithospheric mantle (Black and Liégeois 1993; Abdelsalam et al. 2002; Liégeois et al. 2003) and behaved as a passive continental margin. The Neoproterozoic Iskel block represents the most eastern terrane of Western Hoggar. It is inlaid between the In Tedeini terrane to the west and the LATEA metacraton to the east and it is separated from the latter by the 4°50' shear zone. Caby (2003) considers that Iskel corresponds to a Mesoproterozoic arc-type terrane, showing a low degree metamorphism (greenschist to amphibolite). It is characterized by Neoproterozoic wide magmatic-arc batholiths overlapping the early Neoproterozoic volcano sedimentary series. The presumed Paleoproterozoic granito-gneissic basement outcrop only in the Timgaouine area. Several west-dipping subduction episodes led to the establishment in the middle and in the upper crust of TTG batholiths and typical active margin volcano sedimentary series (Bechiri-Benmerzoug 2009). The 4°50' is considered as a cryptic suture connecting different crustal blocs of LATEA microcontinent and Iskel terrane (Caby 2003) or an internal structure of LATEA, Iskel resting upon the LATEA basement (Azzouni-Sekkal et al. 2003; Liégeois et al. 2003, 2013). At the end of the Pan-African orogeny (during 580–540 Ma) and due to numerous stages of transtension, LATEA and Iskel have been intruded by circular alkali-calcic granitoids called “Taourirt” (Azzouni-Sekkal et al. 2003). Since the Oligocene period, the Tuareg shield has seen an intense volcanic activity due to an asthenospheric upwelling (Dautria and Girod 1991; Aït-Hamou et al. 2000) or to a reactivation of the shield by the distant Africa-Europe convergence (Liégeois et al. 2005). The volcanic activity is represented in several districts (Adrar N'Ajjer, North-Anahéf, South Amadghor, Manzaz, Atakor, Eggéré, In Ezzane, and Tahalgha); some of them follow the North-East South-West oued Amded lineament. The Tahalgha district constitutes the largest volcanic area with 1800 km² and E–W lateral extension across tectonic blocks of LATEA and Iskel terrane. It is composed by extensive basaltic lava (Dautria 1988) issued by several strombolian stratovolcanoes whose volcanic activity started in the Miocene.

The current Hoggar massif is a Precambrian basement of a broad lithospheric swell morphology with a diameter of about 1000 km and an area of ~300,000 km². This asymmetrical dome with a softer slope on the western side, has an altitude of 1000–1500 m and displays volcanic districts whose altitudes

exceed 2000 m (Dautria and Lesquer 1989). Its highest point, Mount Tahat, is located in the Atakor volcanic district at an altitude of 2918 m (Rougier et al. 2013). Based on the modeling of the longitudinal profiles of three major Hoggar oueds, the crustal uplift rate of this massif was estimated by Roberts and White (2010). According to these authors, the uplift began at the Eocene (40–50 Ma) with an amount of 0.2–0.5 km, continued during the Miocene with an amplitude of 0.4–0.6 km. These results are consistent with those obtained from the analysis of the thermochronological data of apatite (U–Th)/He (Rougier et al. 2013). The Hoggar massif as a whole was eroded during the Eocene before the beginning of the magmatic activity at c. 35 Ma. The Hoggar basement that is now exposed on the surface would have been buried after the Early Cretaceous under a sedimentary cover of more than 1 km (Rougier et al. 2013).

In an attempt to study the nature and mantle structure at the origin of this important relief of Hoggar, several geophysical studies have been initiated: using seismic tomography, gravimetric, magnetism, heat flux, and magnetotelluric. Seismic tomography models obtained on a global or continental scale suffer from their low lateral resolution. These models cannot solve geological objects of less than few hundred kilometers in size, such as the different terranes constituting the Hoggar, suture zones or shear zones. However, these tomographic models show a slow and thin lithospheric mantle under the Hoggar relative to the West African Craton in the west, the Saharan metacraton to the east, and the Sahara platform to the north (Sebäi et al. 2006; Priestley et al. 2008; Begg et al. 2009; Fishwick and Bastow 2011; Liégeois et al. 2013). On a local scale, P-wave seismic data confirm that the Hoggar is generally characterized by a slow mantle. More particularly, the volcanic districts of Atakor and Tahalgha are underlain by zones of low seismic velocity in connection with the recent volcanic activity of these districts (Ayadi et al. 2000). On an even smaller scale, around Tamanrasset, Liu and Gao (2010) analyzed the receiver functions obtained at a single station (Geoscope seismic station of Tamanrasset). These authors revealed a Moho at about 34 km below the surface and spatial variations correlated with the rheological characteristics of the crust under the two adjacent terranes. The Tefedest to the west being very fractured contains volcanism, whereas Laouni to the east is less fractured so more rigid, is lacking. The Bouguer anomaly map of the African continent reveals the existence of a negative anomaly in the Hoggar massif (Pérez-Gussinyé et al. 2009). At the Hoggar scale, although the distribution of the data is not perfectly homogeneous and has many gaps, this anomaly appears to be localized in LATEA, more or less coinciding with Atakor, Manzaz, and Amadrar. According to Lesquer et al. (1988), the Hoggar Bouguer anomaly map shows two types of trends: a trend corresponding to the long wavelengths can be correlated with the broad topographic swell, and the other of short wavelengths can be correlated with the structure of the Precambrian basement of the massif. The long wavelength negative anomaly was interpreted as the gravimetric response of a light structure underlying the crust (Lesquer et al. 1988). The effective elastic thickness of the African continent was estimated by Pérez-Gussinyé et al. (2009) from the coherency analysis between the continent topography and the gravimetric data. The Hoggar massif is characterized

by a small effective elastic thickness probably due to a relatively thin lithosphere compared to the West African Craton, the Saharan Metacraton, and the Saharan Platform. Heat flow data show a relatively warm lithosphere in agreement with its Precambrian age with an average of 53 mW/m^2 (Lesquer et al. 1989). A strong anomaly is observed in the north in the Saharan sedimentary basins (Takherist and Lesquer 1989). But an important gap in the data between these two regions does not allow to locate the southern limit of the basins anomaly. However, a relatively important heat flux was observed near Tamanrasset town. It appears to be associated with the Cenozoic magmatic activity of the Atakor and Tahalgha volcanic districts (Lesquer et al. 1989). On the other hand, magnetotelluric data do not show a large-scale regional anomaly under the Hoggar (Bouزيد et al. 2004). Lithospheric conductivity anomalies have been observed that may be associated with some geological faults (Bouزيد et al. 2008) or with volcanic districts such as Atakor (Bouزيد et al. 2015).

3 Data Collection and Analysis

3.1 Data Collection

The magnetotelluric data were collected at 12 sites during two field surveys. Three stations (53, 54 and 55) have been acquired in 2007 during a previously broad reconnaissance survey of Western and Central Hoggar at large scale with $\sim 40 \text{ km}$ interstation distance. The lateral resolution of the MT data was significantly improved by acquiring 9 new sites (1–9) in November 2010. The whole forms an east-west profile 75 km long, centered on the $4^\circ 50'$ mega-fault near Abalessa town, located 70 km west of the city of Tamanrasset (Fig. 2). Another interesting aspect of the MT profile location is that it is located just on the northern flank of the Tahalgha volcanic district. To get a better lateral resolution at the upper crust depth, a 2 km measuring step was adopted near the surface trace of the $4^\circ 50'$ fault. Then, it was increased to 4 , 8 , and 16 km towards the profile ends (Fig. 2). The horizontal telluric (electric) component and the magnetic vector time series have been acquired using the V5 system 2000 of Phoenix Geophysics. To attempt to reach a deep penetration across the lithosphere, each site has been occupied for about 20 h . The measuring sites are located far enough from any significant human activity and electromagnetic noise level was therefore very low, then no reference station was needed. Time series collected have been processed using a robust processing code based on Jones and Jödicke (1984) and provided by the instrument manufacturer. The magnetotelluric impedances and tippers obtained are of good quality and range between periods of 0.001 and 3000 s (Fig. 3). Furthermore, visual examination of apparent resistivity data of the tensor impedance main elements shows no large discrepancy to the very short periods. This offset would be indicative of the presence of static shift, then no such correction was applied to data.

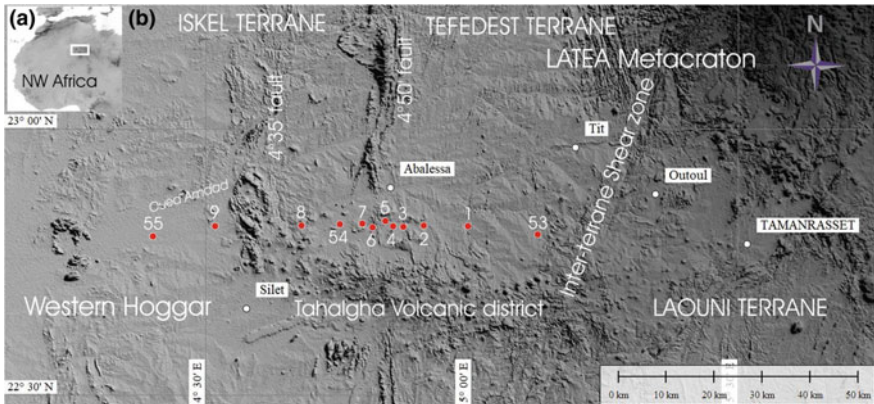


Fig. 2 Location map. **a** A North-West Africa topographic map (GTOPO30), the study area is pointed out by a rectangle. **b** A magnetotelluric sites (dots) location on SRTM3 map of the Silet-Abalessa area. The $4^{\circ}50'$ fault limiting Tefedest terrane from Iskel terrane as well as the $4^{\circ}35'$ fault and the volcanic district of Tahalgha are clearly visible on the topographic map

3.2 Tipper/Induction Vector Data Analysis

The tipper, also called magnetic transfer function, is defined as the ratio of the magnetic field vertical component to its horizontal component. It is theoretically zero for a layered earth but not zero for a 2D or 3D structure. Its magnitude exceeds generally the value of 0.1, sometimes reaches 0.3 at some sites, and is even equal to 0.5 for station 54 at short periods, indicating in these latter cases strong lateral changes in the conductivity distribution in the crust beneath the study area. This was expected if regarding the presence of faults and the vicinity of Tahalgha volcanic district as shown in the geological map (Fig. 1). The induction vector (with its real and imaginary parts) is another way to represent the magnetic transfer function. The real part of the induction vector, plotted in Parkinson's (1962) convention, points towards conductive areas that highly concentrate currents (Fig. 3). Figure 4 shows three maps representing the Parkinson induction vectors plotted for three periods corresponding to three penetration depths: the period of 1/8 s corresponds to upper crust penetration depth, that of 8 s to the lower crust and that of 512 s to the lithospheric upper mantle. For shorter periods, induction vectors are sensitive to local structures. They therefore indicate directions changing from site to another. They point towards two zones in the short period data (1/64–1/8 s): the $4^{\circ}50'$ fault zone close to the center of the profile and another area situated west of station 54 that may be associated with the $4^{\circ}35'$ fault. Although in the latter case, the situation is less obvious due to the larger measuring step. Directions indicated by induction vectors at long periods ($T > 1$ s) are NNW to North and then NNE for longest periods revealing a regional conductive structure located north to NE of the MT profile (Fig. 4). This effect is due to the existence of a lithospheric zone of

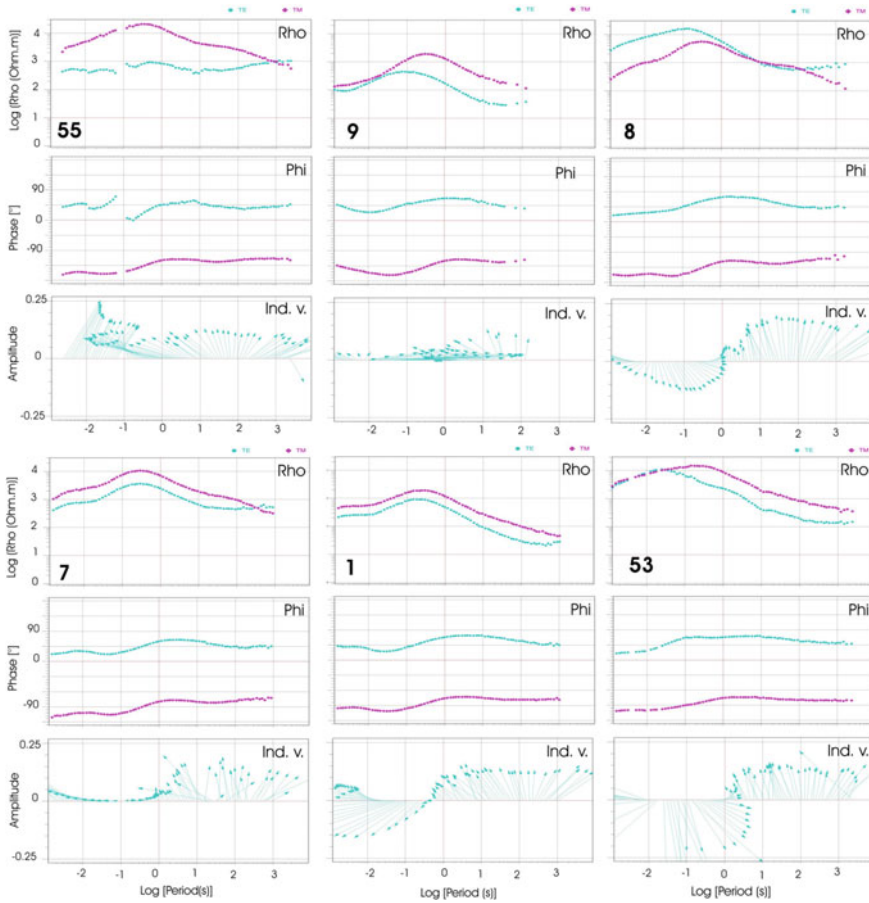


Fig. 3 TE and TM mode apparent resistivity (Rho) and phase (Phi) data, and real component of the induction vector (Ind. v.) plotted following Parkinson's (1962) convention corresponding to sites 55, 9, 8, 7, 1, and 53, respectively. TE and TM mode data are extracted using Groom and Bailey (1989) tensor decomposition for a fixed strike of N15°E

enhanced conductivity that is located out of the profile and which cannot be modeled by these MT sounding data.

3.3 Impedance Tensor Analysis (Dimensionality, Strike)

The magnetotelluric impedance tensor analysis consists in determining the geoelectric structure geometry (or dimensionality) and the direction of the regional structure elongation (strike) if the latter is two-dimensional (2D). This task could

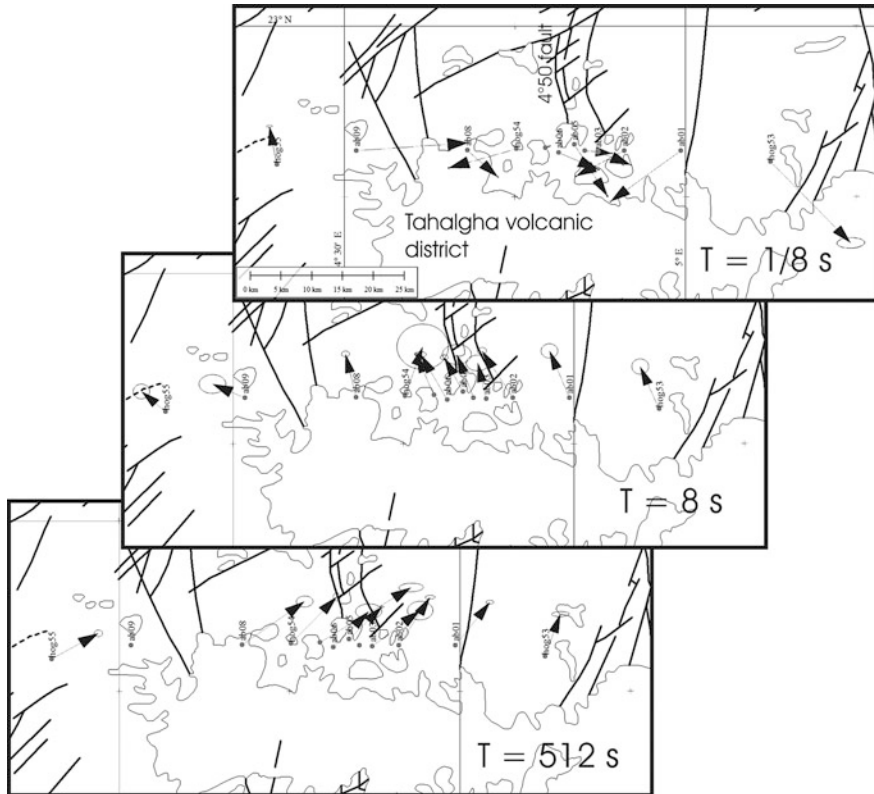


Fig. 4 Induction vectors (Parkinson 1962) maps plotted for three periods corresponding to three different investigation depths. In short and medium periods ($T = 1/8 \text{ s}$), induction vectors point towards two specific area situated beneath the profile: the $4^{\circ}50'$ and the $4^{\circ}35'$ faults. At longer periods, lateral effects are situated north ($T = 8 \text{ s}$) and NE ($T = 512 \text{ s}$) from the MT profile

present some difficulties because the effect of near-surface small-scale inhomogeneities, considered as a geological noise by Bahr (1991), could distort the magnetotelluric response of the regional studied structure. The impedance tensor data analysis was performed according to the method of Bahr (1991) and then that of Caldwell et al. (2004). The Bahr's method consists in determining the values of four dimensionality indicators relative to respective empirical threshold values. The phase-sensitive skew of Bahr (1991) that is sensitive to the geometry of the regional structure only becomes strong (greater than 0.3 or 0.35) for a regional 3D structure. The Bahr skew, calculated frequency by frequency for all stations, remains mainly less than the threshold value of 0.3 (Fig. 5). This indicates that the regional structure under the magnetotelluric profile is roughly not 3D. On the contrary, the Swift (1967) skew, which can be strongly affected by the presence of distortion, exceeds the 0.06 threshold value (Marti et al. 2005) even if the regional structure is 2D or 1D. In the case of our data, this parameter is well above the threshold value

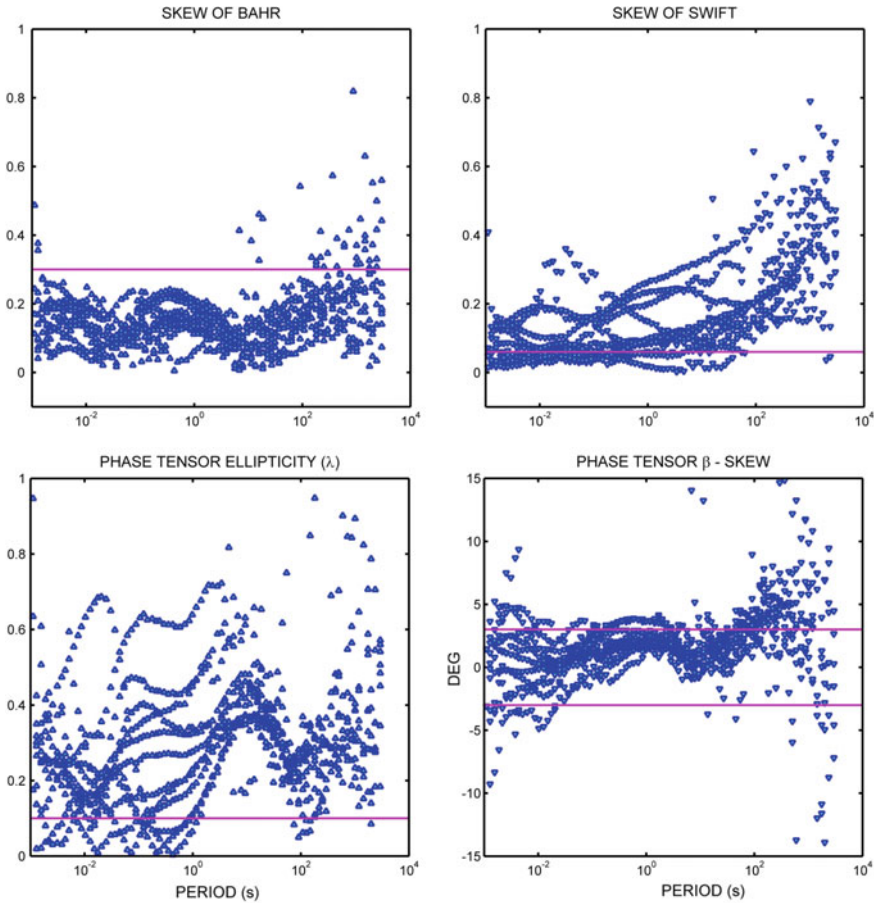


Fig. 5 Phase-sensitive skew (η , Bahr 1991) calculated frequency by frequency for the entire soundings. The line at 0.3 represents an empirical threshold that discriminates between a complex 3D structure ($\eta > 0.3$) and a simple 1D or 2D structure ($\eta < 0.3$). In the figure, some points above the empirical threshold represent a dispersion due to noise in data. The Swift Skew is sensitive to the effect of the galvanic distortion of superficial heterogeneities and may exceed the threshold of 0.06 even if the regional structure is 1D or 2D. Below, the ellipticity of the phase tensor indicates a non-1D structure. The β -skew indicates a roughly 2D regional structure

(Fig. 5). Having a weak Bahr skew concomitantly with strong Swift skew can be interpreted by the existence of a 1D or 2D regional structure to which are superimposed small superficial heterogeneities below the MT data resolution. To determine more accurately the regional structure geometry (i.e., 1D or 2D), it is necessary to call the other two Bahr's parameters, namely the rotationally invariant measure of two dimensionality (Σ) and the regional 1D indicator (μ). These two parameters were calculated systemically for all frequencies and for the entire MT stations. Their analysis site by site shows that the regional structure beneath the MT

profile is 2D with a 3D superficial superimposed inhomogeneities, i.e., 3D/2D structure.

Bahr's analysis was corroborated by that of Caldwell et al. (2004), commonly referred to as the phase tensor method. The phase tensor is defined by the ratio of the imaginary component to the real component of the magnetotelluric impedance tensor (Caldwell et al. 2004; Bibby et al. 2005). Thus, it reflects the regional geoelectric structure without being sensitive to the presence of surface inhomogeneities. The ellipticity (λ) and β -skew parameters deduced from the phase tensor were calculated and plotted frequency by frequency and station by station (Fig. 5). On the whole, the ellipticity remains well above the threshold value (of 0.1) whereas β -skew remains low overall ($<3^\circ$) except for long period data where it exceeds the threshold value. It is then reasonable to conclude that the magnetotelluric data reveal a regional 2D structure beneath the profile. The values of β -skew (low at short periods and stronger at long periods) can be interpreted by the response of some quasi-2D crustal geological structures which will be 2D at the medium periods but rather 3D at the long periods (Fig. 6). In addition, this effect will be more apparent on the TE mode data than on the TM mode data.

The regional structure being roughly 2D, it is necessary to determine the azimuth of its elongation, commonly known as the strike angle. To this end, we used three different approaches. The strike angle was calculated frequency by frequency for each survey using the least square method of Groom and Bailey (1989) then the

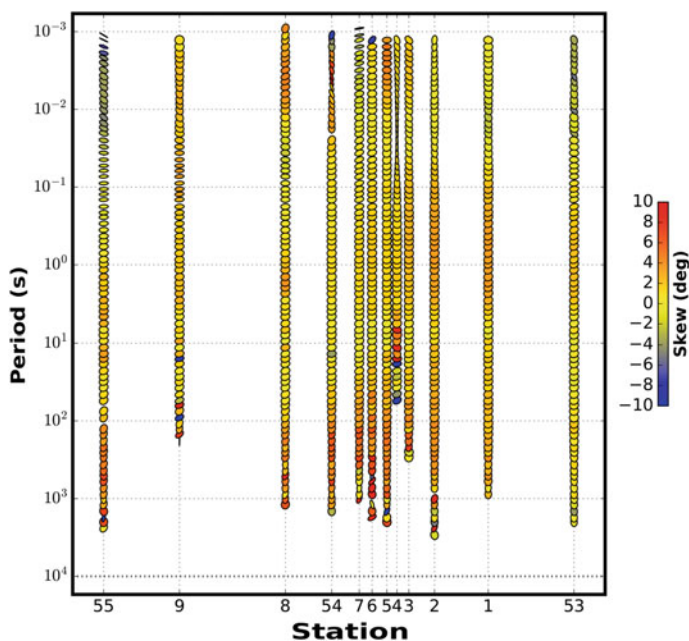


Fig. 6 Phase tensor section plotted using the toolbox of Krieger and Peacock (2014)

analytical formula of Bahr (1988, 1991), and lastly the phase tensor method of Caldwell et al. (2004).

For all three methods, the rose diagrams of the strike angles have been plotted decade by decade to highlight any changes in the strike according to the frequency. This revealed a change in strike at roughly 50 s of period (Fig. 7). Thus, the strike is mainly N15°W for short and medium periods (<50 s) corresponding to crustal depths, and N15°E for long periods (>50 s) corresponding to lithospheric upper mantle penetration (Fig. 7). A difference of 30° in the strike direction is thus shown by MT data between the crust and the mantle.

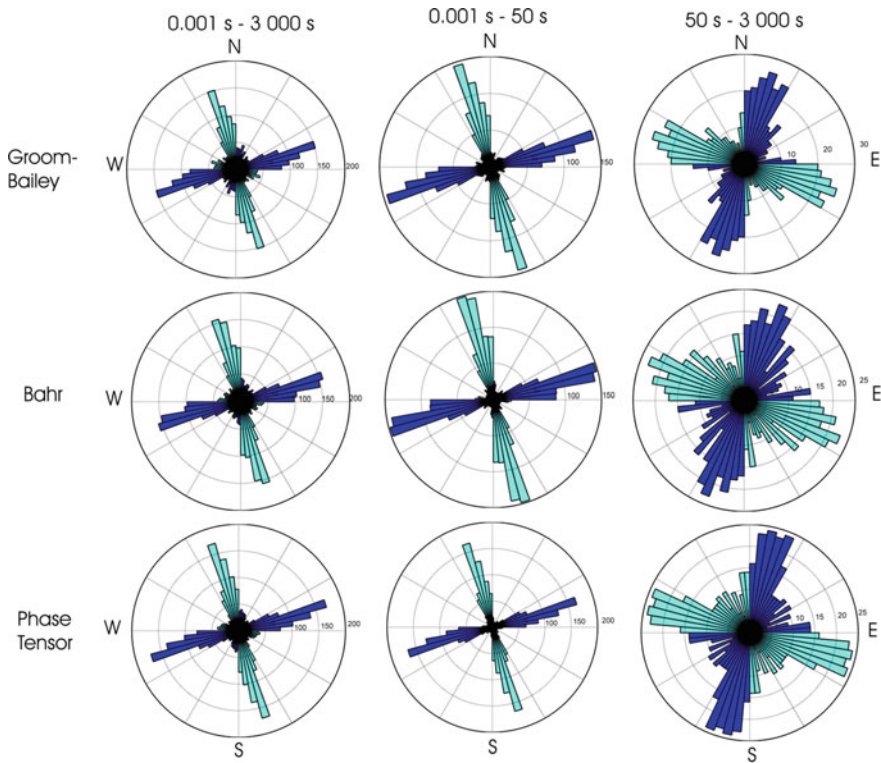


Fig. 7 Strike angles calculated frequency by frequency for all soundings using Groom and Bailey (1991) method (up), Bahr method (middle) and phase tensor method (bottom). The rose diagrams correspond to the entire periods (left column), short and medium periods (in the center) and long period data (right column)

4 Modeling

MT data analysis of all soundings shows a two-dimensional lithosphere structure striking N15°W for short and medium periods that are less than 50 s (crust) and N15°E for long period more than 50 s (lithospheric mantle). Moreover, the measuring site distribution along the profile is not regular. Sites are less spaced at the center (more or less than 2 km) allowing a better resolution of the firsts km of the crust, than at the ends of the profile where the interstation distance increases gradually until reaches 16 km. Taking into account the change in strike according to period and in the measurement step, it seems intuitively more ingenious to model the geoelectric structure under the profile at three different scales: at the central area (at the vicinity of 4°50') with a shallow model, but higher spatial resolution, then at the crustal scale (strike of -15°) and at the lithospheric size (strike +15°).

Once the strike is fixed, the impedance tensor data of each sounding were decomposed using the Groom-Bailey method (1989). TE and TM modes data are then extracted. In all cases, the nonlinear conjugate gradient algorithm of Mackie et al. (1997) implemented in the Geotools package was used to invert the MT data. The algorithm consists in improving by successive iterations a starting model. At each iteration, a new model is calculated by minimizing a functional equal to the linear combination of a measure of the model simplicity (model roughness) and the fit between the model response and the observed data (root mean square or rms). The trade-off between the model roughness and the rms is made by a regularization parameter (τ).

4.1 Modeling Short and Medium Period Data

To model the crustal structure, the strike has been set to N15°W. Indeed, because of the redundancy in the data due to the short measuring step in the central area (only 2 km) and because of the presence of moderate noise in some stations especially to the long period data, three soundings were not used in the inversion, namely stations 4, 6 and 54. A set of 20 periods regularly distributed between 1/560 and 100 s were chosen to achieve the inversion. Several tests were conducted to find the best mesh that gives the lowest root mean square (rms). Then, a study was conducted to determine the optimum value of the regularization parameter (τ) that plays a role as a balance between data (rms) and the simplicity of the solution (model roughness). Thus, several inversions were performed by changing the τ value from 1, 2, 3, etc., to 100, while keeping the remainder unchanged. For each rms value, the model roughness is plotted with respect to the inverse of τ (Fig. 8). Three L-curves are therefore obtained in the case of the inversion of the TE mode data only, the TM mode data only and simultaneously both modes data (Hansen 1992). They provide three different optimum values of τ parameter, which are, respectively, 8, 10, and 8 (Fig. 8). At this stage, the inversion of apparent resistivity and

phase data of the TE mode only and the TM mode only was carried out in two steps, by varying the noise floor on the data. This was taken as 50% on the apparent resistivity data and 2.87° on the phase data (equivalent to 5% on impedance). Then, in the second step, respectively of 10% and 2.87° (Fig. 9b). On the other hand, the simultaneous inversion of the data of both modes was carried out in two steps. In first step, the TM model previously obtained was used as starting model, with therefore the following noise floor values: 10% and 2.87° for respectively apparent resistivity and phase of the TM mode data, and 50% and 2.87° for those of the TE mode data. Then, in a second step, and for both modes, the error floor on apparent resistivity is fixed to 10% and phase to 2.87° . The 2D model was obtained with an rms of 3.67. A similar approach was followed to invert data of both modes but by taking TE 2D model previously calculated as initial model. The resultant model was obtained with an rms of 4.01.

The MT data show that the crustal structure is more conductive in the NNW direction (TE mode) than in the perpendicular direction (TM mode). As a result, the penetration depths obtained by the TM mode data are larger than those of the TE mode data. On the other hand, the MT sites located directly above conductive structures have a smaller investigation depth because they strongly attenuate the electromagnetic waves. This is clearly shown by the Niblett-Bostick transform. Indeed, for the TE mode data and for periods shortest than 50 s, the depth of investigation is about 40 km under stations 8, 2, and 53 while it does not exceed 15 km under the western part of the profile (under 55 and 9), and 18–25 km under the central part of the profile (5, 6 and 3) and under station 1. These three zones display strong drops in electrical resistivity. In contrast, the penetration depths are more important for the TM mode data. They exceed 40 km except under the center of the profile where they reach 30 km. Moreover, the TE mode data are more sensitive to the 3D effects of off-line structures than those of the TM mode. This explains the higher rms (4.39) in the first case and very acceptable one in the second (rms of 0.77). The geological map of the study area shows precisely the presence of changes in geological structure geometry from 10 to 15 km to the north and south of the MT profile. On the other hand, the model corresponding to the TE mode is more sensitive to thin conductive structures than that of the TM mode, which tends to smooth the structures in the model. This is most likely the case of the conductive body located beneath the central zone clearly indicated by the TE data but not in TM mode.

4.2 Modeling of the Central Area

To improve the spatial resolution of the resistivity model of the near surface crustal structure close to the $4^\circ50'$ fault area, a short profile of 7 stations and 16 km long has been selected. The interstation distance varies from 1.5 to 4 km. The strike was set to -15° (N15°W) then TE and TM mode data were extracted according to the GB method (Groom and Bailey 1989). Apparent resistivity and phase data corresponding to 19 periods ranging from 1/560 to 56 s (frequency of 0.018 Hz) were

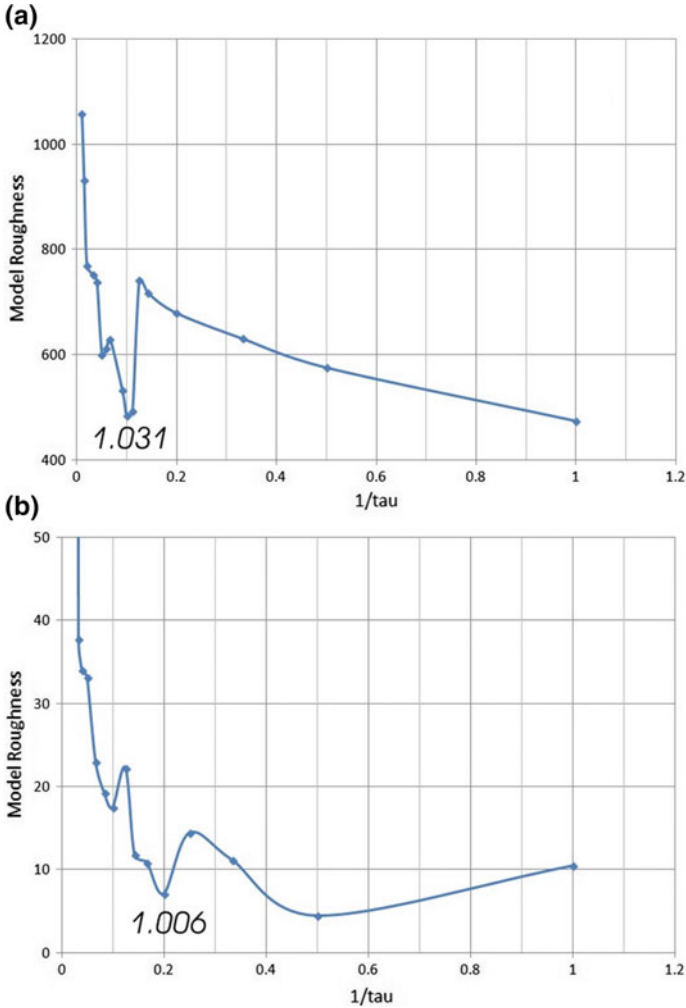


Fig. 8 L-curve representing the model roughness versus the reverse of regularization parameter (τ) for different root mean square (rms) for TM mode data 2D inversion corresponding to short and medium period data of models **a** and **b** in Fig. 9 (top in **a**), and to broadband data of model **c** in Fig. 9 (bottom in **b**). The corner of the curve which gives the optimum value of the regularization parameter corresponds to an rms of 1.031 in the case of the short and medium period data (**a**) and 1.006 in the case of the broadband data (**b**)

chosen to be inverted to estimate the crustal resistivity model. Models corresponding to TE mode only or TM mode only and both modes data were calculated in the same manner than that followed previously for the short and medium data of the previous section. TE model, TM model, TE+TM model (using the obtained TE model as starting model) and TM+TE model (using the obtained TM model as

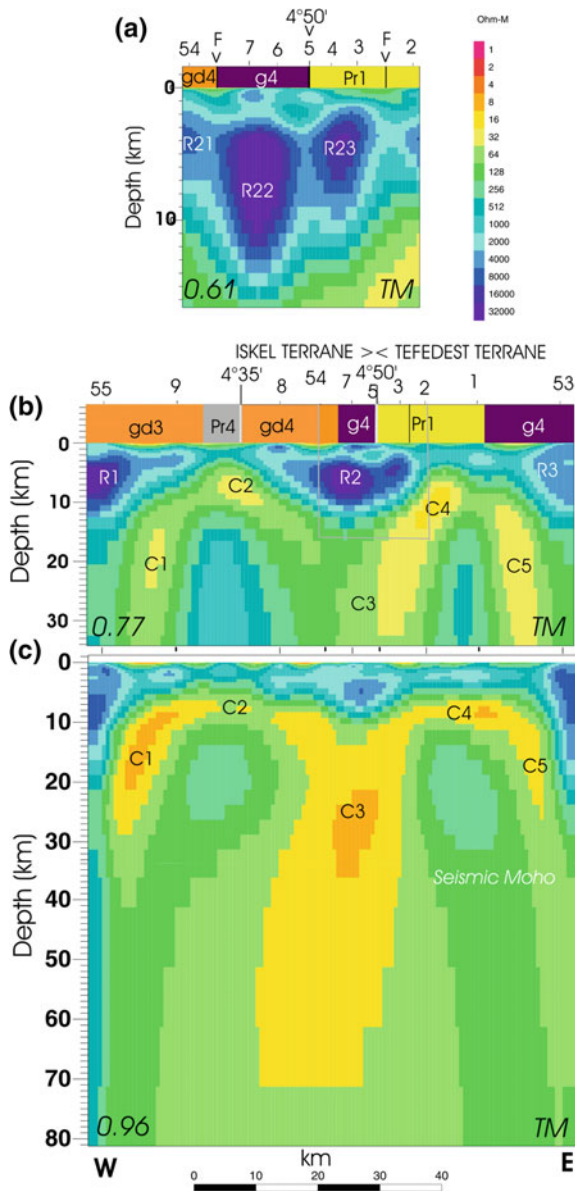


Fig. 9 Crustal 2D resistivity models obtained by inversion of apparent resistivity and phase of TM mode data corresponding to short period and central area, near the 4°50' mega-fault (top in **a**), short and medium period data (in **b**) and broadband data (bottom in **c**). The description of the surface geology (colored bar on the top of the resistivity models of **a** and **b**) was taken from the Hoggar geological map at 1/1,000,000 of Bertrand and Caby (1977). The notations used are as follows: Pr1, for Paleoproterozoic LATEA metacraton basement; g4, for high-K calc-alkaline granitoids (HKCA, 630–580 Ma); Pr4, for Neoproterozoic volcano sedimentary series; gd3 and gd4, for Neoproterozoic granodiorite/calco alkaline granites magmatic province

starting model), were found with respectively the rms values of 4.72, 0.61, 3.85 and 5.47 (TM model is shown on Fig. 9a). TE model reveals mainly a strong conductive structure under site 6 that extends to the surface. However, this conductive structure appears with a much lower contrast on the TM model. It could then be a structure so thin that it is not resolved by TM mode data.

4.3 Modeling of Long Period Data

The same approach was followed for the inversion of the long period data. A significant penetration depth reaching the lithospheric mantle to about 100 km is obtained. The central part of the profile being relatively densely covered only was taken into account stations with good quality data. Thus, 8 stations were used in the inversion, namely, 55, 9, 8, 54, 5, 2, 1, and 53. The strike was set to N15°E and the Groom-Bailey TE and TM modes data were extracted from the measured tensor (Groom and Bailey 1989). The study of the regularization parameter τ gives the following values: 9 for the TE mode data, 5 for the TM mode data, and 7 for data of both modes (Fig. 8). Furthermore, 23 periods were used that are regularly distributed between 1/320 and 1000 s. The inversion process produces solutions with an rms of 5.82 for the TE mode data only, 0.96 for the TM mode data only, 4.93 for both modes data with TM model used as starting model, and 4.47 for that using TE model as starting model (Fig. 9c for TM model). The last two models are very similar to the TE model and do not provide more information especially for the deeper part. As the strike change occurs around 50 s, a modeling was performed for the long period data with a strike of -15° (as was the case for short and medium periods). The models obtained give a better definition of the crustal part (which is similar to the models obtained for short and long periods) but a very poor resolution for the deep structure (homogeneous model without a change in the resistivity) with however stronger rms. Due to a drop in electrical resistivity in some parts of the crust, the TE mode data penetration does not exceed 15 km under station 9, while it is about 60 km under station 1. For TM mode data, a relatively shallow penetration is obtained under stations 2 and 9 (approximately 70 km). Everywhere else, the depth of investigation reaches 100 km depth or more.

2D models corresponding to TE mode data were obtained with relatively strong rms (>4 in all cases). This is because TE mode data remains very sensitive to 3D effects and unlike those of TM mode. However, the latter give resistivity models with a very acceptable rms but having rather smooth structures. For this purpose, the resistivity models calculated from the TM mode data only have been selected for geological interpretation (Fig. 9).

5 Gravimetric and Aeromagnetic Data Constraints

The constraints provided by the gravimetric and magnetic data are complementary to those of the MT data. Indeed, the potential methods have a better lateral resolution than the MT, while the latter being a probing method better resolves the depths of the geological layers. Potential field data available in the study area will be analyzed and modeled. The results obtained will be integrated with those of magnetotellurics.

The gravimetric data processed in this study come from a compilation of data from several old gravimetric surveys to which new data are added. The new data were collected during a field survey carried out in 2005 along a profile from Tamanrasset to Silet. These new data, linked to the Algerian absolute measurement network, made it possible to homogenize the data of the different surveys (Bouyahiaoui et al. 2011). Their measurement accuracy is of the order of 0.5 mgal. The distribution of the measurement points is inhomogeneous, but a large part of the points is concentrated in the center of the map with an equidistance of about 2 km. The Bouguer anomaly was calculated on the basis of a correction density of 2.67 and a topographic correction at a distance of 110 km (Fig. 10). The gravimetric anomaly map (Fig. 10a) shows that anomalies with an amplitude greater than 40 mgals are elongated in an NS direction. The central area of the map is characterized by a negative anomaly almost wedged between positive anomalies, which suggests a mass deficit in the region centered on the 4°50' fault. The vertical gradient map (Fig. 10b) enhances the high frequencies and highlights the gravimetric anomalous axes and contacts. It shows a succession of positive and negative anomalies, elongated in the NS direction, revealing the presence of faults within the crust. Thus, the 4°50' fault signature can be highlighted (Fig. 10).

The magnetic data come from an aero-geophysical survey covering the entire Algerian territory and carried out in 1971 by the American company AERO-SERVICE CORPORATION (ASC). The direction of the flight plans is oriented in EW. The distance between the flight lines is 2 km. It is however 40 km for the tie lines. On a flight line, a measurement is taken every 50 m. The flight altitude is kept constant at 150 m (Bournas et al. 2003). Moreover, the reduced to the pole magnetic map (Fig. 11a) is dominated by a large positive anomaly covering the entire central part of the map. This strong anomaly superimposed rather well with the Tahalgha volcanic district corresponds to the magnetic signature of the lava field. It therefore partly hides the rest of the nearby magnetized geological formations. The vertical gradient map (Fig. 11b) makes it possible to reduce the effect of the lava and to highlight several magnetic discontinuities, as is the case of the positive magnetic anomaly of NS elongation and corresponding to 4°50' fault.

The gravimetric and magnetic data along a profile that coincides with the MT stations were inverted jointly using GEOSOFT's GMSYS routine. The 2D model (Fig. 12) obtained shows that the lower crust thickens at the center of the profile under the 4°50' fault to reach a depth of 43 km. Then, the Moho rises to a depth of 22 km to the west end and 30 km to the east end. The lower crust is bordered by

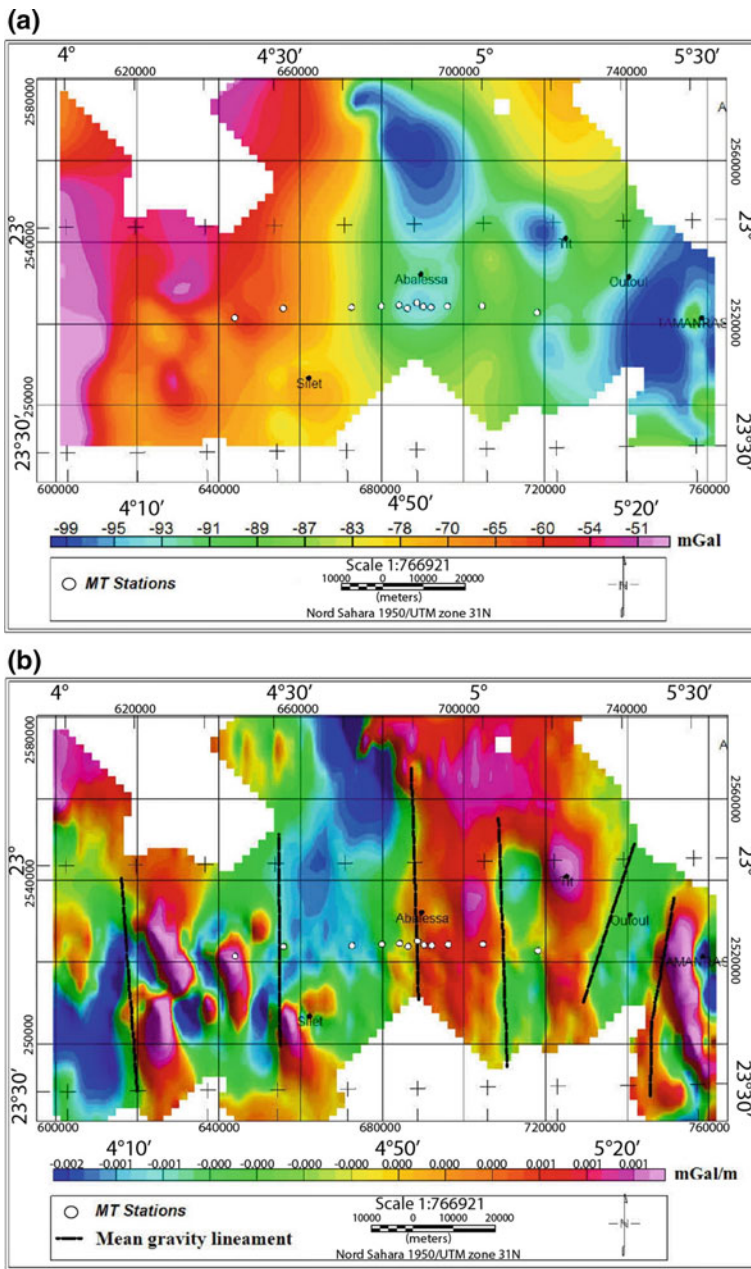


Fig. 10 Bouguer anomaly map around the study area (a) and that of its vertical derivative (b)

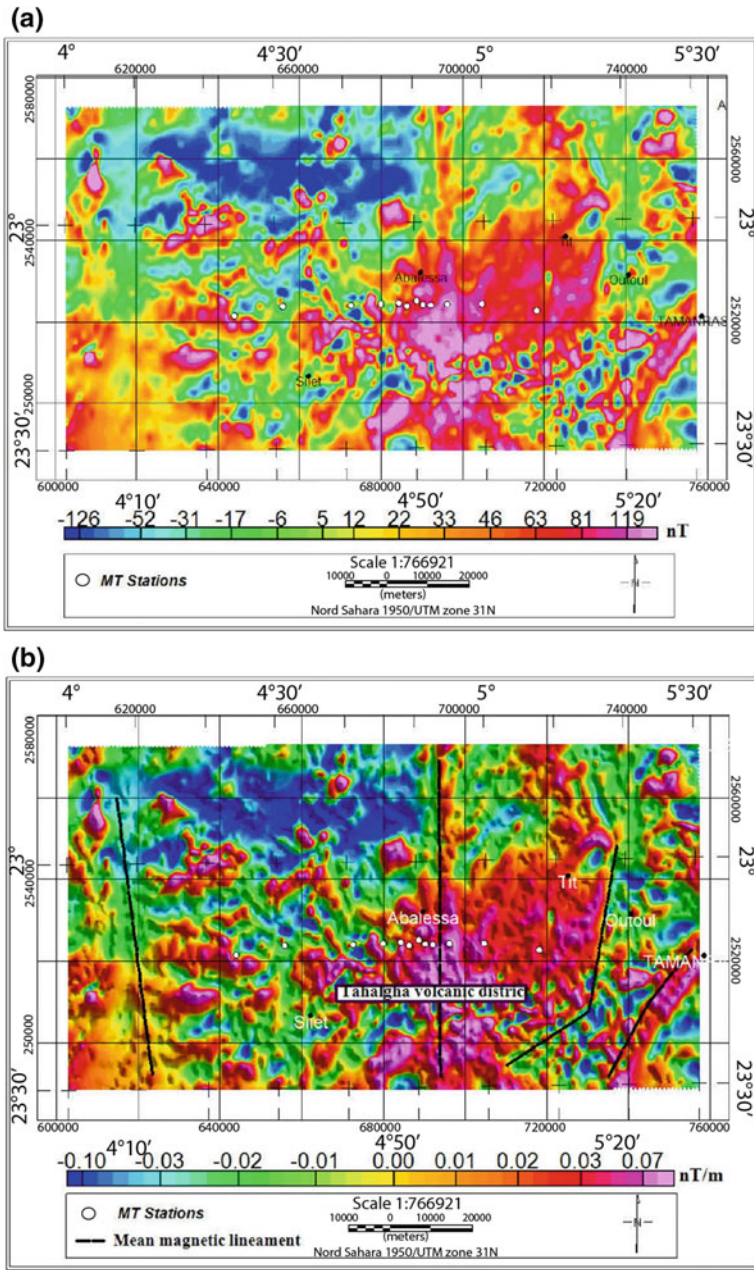


Fig. 11 Aeromagnetic map around the study area (a) and that of its vertical derivative (b)

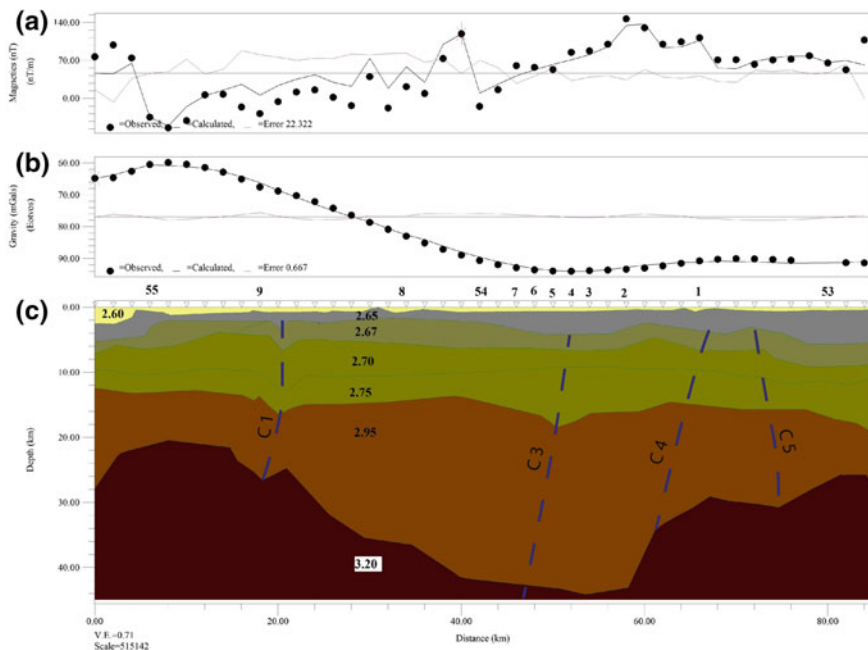


Fig. 12 Joint inversion of gravimetric and aeromagnetic data. **a** Misfit between observed magnetic data and magnetic response of the model shown in **c**. **b** Misfit between observed gravimetric data and gravimetric response of the model shown in **c**. **c** Model obtained by joint inversion of both data types

two discontinuities and is crossed by two faults. The upper crust of almost constant thickness reaches a depth of the order of 14 km.

6 Geological Interpretation

The magnetotelluric data acquired on the LATEA western boundary near Tahalgha volcanic district show a mainly two-dimensional lithosphere with a structure elongation in N15°W direction for the crust, and N15°E for the underlying lithospheric mantle. At the scale of the study area, the N15°W strike is supported by the local surface trace directions of the major faults affecting the study area (4°50', 4°35' faults). By contrast, the N15°E structural direction observed in the lithospheric mantle do not correlate with surface geological structures (Fig. 2). Taking into account the non-regular distribution of the MT sites, with a short measuring step in the center (up to 2 km) but wide towards the profile ends and the strike change with the depth, on the other hand, we calculated three resistivity models at three different scales (Fig. 9). A lithospheric model reaching an 80 km depth (Fig. 9c), then a

crustal model (Fig. 9b) and lastly a high-resolution model of the central area around the 4°50' fault (Fig. 9a). From depth to the surface, these three resistivity models show a fairly homogeneous lithospheric mantle with a resistivity of 100–200 Ωm . The lithospheric mantle contains a subvertical conductor rooted down to a depth of about 70 km and ascending to the base of the upper crust. This conductor, reaching a width of 10–20 km, perhaps less because it may appear more spread due to a loss in resolution with depth inherent to the magnetotelluric technique, is located directly below the 4°50' fault (C3, Fig. 9). However, the model does not show any change in resistivity at the Moho depth, estimated at about 34 km below the surface by the analysis of the receiver functions obtained at the GEOSCOPE station at Tamanrasset (Fig. 9c). On the other hand, a very inhomogeneous upper crust is revealed. This modeled upper crust has an excellent correlation with the surface geology (Fig. 9b). From the crustal resistivity model, one can discern some crustal blocks corresponding to batholiths (R1, R2, and R3, Fig. 9b), characterized by a very resistive upper crust ($>10,000 \Omega\text{m}$) and others corresponding to the Paleoproterozoic metamorphic basement, much less resistive (C2 and C4, Fig. 9b). In the vicinity of the 4°50' fault, the central area of about 20 km lateral width is underlain by a relatively conductive middle and lower crust of about 100 Ωm (C3, Fig. 9b). But, at both profile ends, particularly under the metamorphic blocks of the Paleoproterozoic and late Neoproterozoic metamorphic basement, the crustal resistivity is relatively larger reaching a resistivity of about 500 Ωm (C2 and C4, Fig. 9b). These two portions of the crust are crossed by subvertical faults that are rooted in the crust.

The magnetotelluric profile spreads over the western edge of LATEA which is an old craton remobilized during the Pan-African Orogeny. At the scale of the studied area, the Tefedest terrane is characterized by a Polycyclic Paleoproterozoic gneissic basement (Pr1) that is intruded by (630–580 Ma) HKCA granitoids (g4) at the eastern edge of the profile. The two crustal blocks are separated by an intra-terrane sub-meridian shear zone of N10°E direction at the local scale (Fig. 1). The magnetotelluric model reveals a resistive ($>10,000 \Omega\text{m}$) upper crust below Tefedest terrane of about 15 km thick beneath the Pan-African batholith of Tit (R3, Fig. 9b; see Fig. 2) to the east, and <10 km thick under the Paleoproterozoic metamorphic basement to the west (C4, Fig. 9b). The intra-terrane shear zone separating the two latter crustal portions, probably having played an important role in the HKCA batholith emplacement during the Pan-African Orogeny, is underlain by a subvertical conductor that reaches at least the base of the crust (C5, Fig. 9b). This conductive body could be interpreted as the electrical signature of a shear zone within the upper crust as shear zones often causes a decrease in the electrical resistivity due to an increase in porosity and to the presence fluids or mineralization in the pores.

The western part of the MT profile is located on the Iskel thrust terrane whose crust seems to be more inhomogeneous and complex with several conductive and resistive crustal portions as might be expected from the surface geology and the geologic history of this island arc (Fig. 9b). From the resistivity model, we can discern from east (near 4°50' fault) to west, three crustal entities: a thick granitoid

batholith probably the continuation of Anou-Eheli (640 Ma) batholiths (Bechiri-Benmerzoug 2009), rooted in the base of the upper crust (R2, Fig. 9b), a conductive block corresponding to a metagreywakes formation limited to the east by a $4^{\circ}35'$ sub-meridian fault (C2, Fig. 9b), and to the west a resistive block representing a thick Neoproterozoic batholiths (R1, Fig. 9b).

The mega-shear zone commonly known as $4^{\circ}50'$ fault limiting the Tefedest terrane (LATEA) to the east from the Iskel terrane (Western Hoggar) to the west, is clearly evidenced by the MT data (Fig. 9). It corresponds to a conductive sub-vertical body of 10 km width or more in the lower crust and upper mantle (C3, Fig. 9b and c) but only of few kms width near the surface where it joins the $4^{\circ}50'$ trace at the surface (Fig. 9a). This change in width with depth could be explained by the rheological behavior of the crust near the Abalessa area. Indeed, in the upper crust, the $4^{\circ}50'$ fault is sharp when it crosses the thick, resistive, and compact batholith, whose behavior is rather rigid (Fig. 9a). At the lithospheric scale, its signature is evident to a depth of several tens of kilometers. This fault appears to be connected with the conductive structures C2 and C4 (Fig. 9b and c) of the middle crust beneath the studied area. The loss in resolution of the method in the deep lithosphere does not make it highlighted to these depths (Fig. 9c). The model obtained by joint inversion of potential data (Fig. 12) is in agreement with the resistivity model (Fig. 9b). Unlike the case of $4^{\circ}50'$, the resistivity model shows that the fault of $4^{\circ}35'$, located inside the Iskel terrane, is not associated with any deep conductor. This is corroborated by the potential data model. Consequently, the $4^{\circ}50'$ appears as the major fault in the area, with a deep root in the lithospheric mantle.

The MT profile is located just on the northern flank and parallel to the Tahalgha volcanic district which extends in the E–W direction. Some stations are located even near or at some kilometers from volcanoes. The Pan-African structure, especially the various crustal faults and the fragile zones of the upper crust which correspond to conductive structures on the resistivity model, has certainly allowed the transport of melt from asthenosphere to surface. Fluids released by the magma and/or the precipitation of mineralization give rise to strong drops in the resistivity. In the absence of other constraints, the resistivity model cannot clearly state whether this signature corresponds to a Pan-African heritage, or to the Cenozoic reactivation. On another side, the relatively short length of the MT profile (~ 75 km) with respect to the width of the oued Ameded lineament (see Fig. 1) does not make it possible to constrain the lithospheric structure of this important geological object.

7 Conclusions

The crustal and upper mantle structure of the Hoggar massif is the subject of hot scientific debates because it remains relatively unknown. Indeed, the lack of high-resolution geophysical studies in the region allows discrepancies between the

various hypotheses formulated on the structure and deep nature of the Hoggar massif. In the present study, magnetotelluric was used to constrain the lithospheric geological structure of the Abaessa region, located on the LATEA western boundary. The study area is geologically complex because it is located at the intersection of the 4°50' major fault with the oued Ameded lineament, and on the northern flank of the Tahalgha volcanic district.

The collection of nine magnetotelluric sites added to three former sites belonging to a reconnaissance campaign allowed to model the crustal and upper mantle structure down to a hundred kilometers depth. Magnetotelluric data reveal crustal structures striking N15°W. This direction changes on 30° in the lithospheric mantle to be at N15°E. The resistivity model obtained by inversion of magnetotelluric data shows a rather inhomogeneous upper crust. The latter is made up of probably very compact and strong, electrically resistive structures corresponding to granitoids and batholiths, and others more conductive probably more inhomogeneous, weaker and more fractured corresponding to the Paleoproterozoic metamorphic basement. On the contrary, the lower crust and the lithospheric mantle down to a depth of about 100 km are fairly homogeneous.

The signature of some important faults is apparent at the crustal scale. Beneath the eastern side of the MT profile, the fault separating the Tit batholith (g4) to the east from the Proterozoic basement to the west can be discerned (Pr1, Fig. 9). In the profile on the western side, another crustal fault underlays the shallow batholith. The relatively short profile size makes it impossible to check whether these two faults are connected to others. The most important electrical signature is that of the 4°50' fault which appears to extend into the lithospheric mantle to a depth of about 70 km. This is corroborated by the potential field data showing a root for the 4°50' fault to at least the base of the crust. Near the surface and in the upper crust, this fault is relatively thin because it crosses a rigid medium. At depth, it becomes wider due to a lower ductile crust. On the other hand, the fault 4°35' is not as deep. The fault network highlighted by the magnetotelluric model has probably been used to transport melt from the asthenosphere up to the surface to give rise to the Tahalgha volcanic district. The fluids released or the precipitated mineralization are at the origin of the strong fall of the resistivity which gives a so peculiar signature to these faults. The results obtained in this study will be more thorough during other magnetotelluric surveys planned soon in this area of the Hoggar massif.

Acknowledgements This study was conducted in the framework of the Algerian/French PHC Tassili cooperation program n° 09 MDU 787: « architecture et evolution du Bouclier Touareg: le rôle des grands accidents lithosphériques ». The field campaign was carried out with the support of CRAAG. We thank M. Hani for his help during the fieldwork. The civil and military authorities of the Wilaya of Tamanrasset are thanked for their assistance in achieving the field campaign. The authors are grateful to A. Bendaoud, J.-L. Bodinier, C. Tibéri, A. Lesquer, and G. Vasseur for their fruitful discussions about this work. We warmly thank Prof. J.-P. Liégeois for his constructive criticism that has resulted in a substantial improvement of the manuscript.

References

- Abdelsalam M, Liégeois J-P, Stern RJ (2002) The Saharan metacraton. *J Afr Earth Sci* 34:119–136. [https://doi.org/10.1016/S0899-5362\(02\)00013-1](https://doi.org/10.1016/S0899-5362(02)00013-1)
- Aït-Hamou F, Dautria JM (1994) Le magmatisme cénozoïque du Hoggar: une synthèse des données disponibles. Mise au point sur l'hypothèse d'un point chaud. *Bull Serv Géol Algérie* 5:49–68
- Aït-Hamou F, Dautria JM, Cantagrel JM, Dostal J, Briquieu L (2000) Nouvelles données géochronologiques et isotopiques sur le volcanisme cénozoïque de l'Ahaggar (Sahara algérien): des arguments en faveur d'un panache. *C R Acad Sci Paris* 330:829–836
- Ayadi A, Dorbath C, Lesquer A, Bezzeghoud M (2000) Crustal and upper mantle velocity structure of the Hoggar swell (central Sahara, Algeria). *Phys Earth Planet Inter* 118:111–123. [https://doi.org/10.1016/S0031-9201\(99\)00134-X](https://doi.org/10.1016/S0031-9201(99)00134-X)
- Azzouni-Sekkal A, Liégeois J-P, Bechiri-Benmerzoug F, Belaidi-Zinet S, Bonin B (2003) The 'Taourirt' magmatic province, a marker of the closing stage of the Pan-African orogeny in the Tuareg Shield: review of available data and Sr–Nd isotope evidence. *J Afr Earth Sci* 37:331–350
- Bahr K (1988) Interpretation of the magnetotelluric impedance tensor: regional induction and local telluric distortion. *J Geophys* 62:119–127
- Bahr K (1991) Geological noise in magnetotelluric data: a classification of distortion types. *Phys Earth Planet Inter* 66:24–38. [https://doi.org/10.1016/0031-9201\(91\)90101-M](https://doi.org/10.1016/0031-9201(91)90101-M)
- Bechiri-Benmerzoug F (2009) Pétrologie, géochimie isotopique et géochronologie des granitoïdes Pan-africains de type TTG de Silet: contribution à la connaissance de la structuration du bloc d'Iskel (Silet, Hoggar occidental). Doctoral dissertation, USTHB/FSTGAT, Algeria, 335 p
- Begg GC, Griffin WL et al (2009) The lithospheric architecture of Africa: seismic tomography, mantle petrology and tectonic evolution. *Geosphere* 5:23–50
- Bendaoud A, Ouzegane K, Godard G, Liégeois J-P, Kienast J-R, Bruguier O, Drareni A (2008) Geochronology and metamorphic P-T-X evolution of the Eburnean granulite-facies metapelites of Tidjenouine (Central Hoggar, Algeria): witness of the LATEA metacratonic evolution. In: Ennih N, Liégeois J-P (eds) The boundaries of the West African craton. Geological Society of London Special Publication, vol 297, pp 111–146. <https://doi.org/10.1144/sp297.6>
- Bertrand JM, Caby R, SONAREM Geologists, Compilers (1977) Carte géologique du Hoggar (Algeria). SONAREM, Algiers, scale 1:1,000,000, 2 sheets
- Bibby HM, Caldwell TG, Brown C (2005) Determinable and non-determinable parameters of galvanic distortion in magnetotellurics. *Geophys J Int* 163:915–930. <https://doi.org/10.1111/j.1365-246X.2005.02779.x>
- Black R, Liégeois J-P (1993) Cratons, mobile belts, alkaline rocks and continental lithospheric mantle: the Pan-African testimony. *J Geol Soc* 150:89–98. <https://doi.org/10.1144/gsjgs.150.1.0088>
- Black R, Latouche L, Liégeois JP, Caby R, Bertrand JM (1994) Pan-African displaced terranes in the Tuareg shield (central Sahara). *Geology* 22:641–644. [https://doi.org/10.1130/0091-7613\(1994\)022%3c0641:padtit%3e2.3.co;2](https://doi.org/10.1130/0091-7613(1994)022%3c0641:padtit%3e2.3.co;2)
- Bourmas N, Galdeano A, Hamoudi M, Baker H (2003) Interpretation of the aeromagnetic map of Eastern Hoggar (Algeria) using the Euler deconvolution, analytic signal and local wavenumber methods. *J Afr Earth Sci* 37:191–205
- Bouyahiaoui B, Djeddi M, Abtout A, Boukerbout H, Akacem N (2011) Etude de la croûte Archéenne du môle In-Ouzzal (Hoggar Central) par la méthode gravimétrique: identification des sources par la transformée en ondelettes continue. *Bull Serv Géol Nat* 22(2):259–274
- Bouzid A, Abtout A, Akacem N (2004) Electrical structure of the crust and upper mantle of the Hoggar shield from magnetotelluric data. In: Proceedings, 20th colloquium of African geology, Orléans, France, Abstracts, p 93

- Bouid A, Akacem N, Hamoudi M, Ouzegane K, About A, Kienast J-R (2008) Modélisation magnétotellurique de la structure géologique profonde de l'unité granulitique de l'In Ouzal (Hoggar occidental) [in French with an abridged English version]. *C R Geosci* 340:711–722. <https://doi.org/10.1016/j.crte.2008.08.001>
- Bouid A, Bayou B, Liégeois J-P, Bourouis S, Bougchiche SS, Bendekken A, About A, Boukhlof W, Ouabadi A (2015) Lithospheric structure of the Atakor metacratonic volcanic swell (Hoggar, Tuareg Shield, southern Algeria): electrical constraints from magnetotelluric data. In: Foulger GR, Lustrino M, King SD (eds) *The interdisciplinary earth: a volume in honor of Don L. Anderson*. Geological Society of America Special Paper 514 and American Geophysical Union Special Publication 71, pp 239–255. [https://doi.org/10.1130/2015.2514\(15\)](https://doi.org/10.1130/2015.2514(15))
- Caby R (2003) Terrane assembly and geodynamic evolution of central-western Hoggar: a synthesis. *J Afr Earth Sci* 37:133–159
- Cagniard L (1953) Principe de la méthode magnétotellurique, nouvelle méthode de prospection géophysique. *Ann Geophys* 9:95–125
- Caldwell TG, Bibby HM, Brown C (2004) The magnetotelluric phase tensor. *Geophys J Int* 158:457–469. <https://doi.org/10.1111/j.1365-246X.2004.x>
- Crough ST (1981) Free-air gravity over the Hoggar massif, northwest Africa: evidence for the alteration of the lithosphere. *Tectonophysics* 77:189–202. [https://doi.org/10.1016/0040-1951\(81\)90262-6](https://doi.org/10.1016/0040-1951(81)90262-6)
- Dautria J-M (1988) Relations entre les hétérogénéités du manteau supérieur et le magmatisme en domaine continental distensif. Exemple des basaltes alcalins du Hoggar (Sahara central, Algérie) et de leurs enclaves. Ph.D. thesis. Université de Montpellier 2, 421 p
- Dautria JM, Girod M (1991) Relationships between Cainozoic magmatism and upper mantle heterogeneities as exemplified by the Hoggar volcanic area (Central Sahara, South Algeria). In: Kampunzu AB, Lubala RT (eds) *Magmatism in extensional structural settings*, Springer, Berlin, pp 250–269
- Dautria JM, Lesquer A (1989) An example of the relationship between rift and dome: recent geodynamic evolution of the Hoggar swell and of its nearby regions (Central Sahara, Southern Algeria and Eastern Niger). *Tectonophysics* 163:45–61. [https://doi.org/10.1016/0040-1951\(89\)90117-0](https://doi.org/10.1016/0040-1951(89)90117-0)
- Dautria JM, Dostal J, Dupuy C, Liotard JM (1988) Geochemistry and petrogenesis of alkali basalts from Tahalra (Hoggar, Northwest Africa). *Chem Geol* 69:17–35. [https://doi.org/10.1016/0009-2541\(88\)90155-6](https://doi.org/10.1016/0009-2541(88)90155-6)
- Fishwick S, Bastow ID (2011) Towards a better understanding of African topography: a review of passive-source seismic studies of the African crust and upper mantle. In: van Hinsbergen DJJ, Buiter SJH, Torsvik TH, Gaina C, Webb SJ (eds) *The formation and evolution of Africa: a synopsis of 3.8 Ga of earth history*. Geological Society of London Special Publication, vol 357, pp 343–371. <https://doi.org/10.1144/sp357.19>
- Gangopadhyay A, Pulliam J, Sen M-K (2007) Waveform modeling of teleseismic S, Sp, SsPmP, and shear-coupled PL waves for crust- and upper-mantle velocity structure beneath Africa. *Geophys J Int* 170:1210–1226. <https://doi.org/10.1111/j.1365-246X.2007.03470.x>
- Gokarn SG, Gupta G, Rao CK, Selvaraj C (2002) Electrical structure across the Indus Tsangposuture and Shyok suture zones in NW Himalaya using magnetotelluric studies. *Geophys Res Lett* 29(8):1251. <https://doi.org/10.1029/2001GL014325>
- Groom RW, Bailey RC (1989) Decomposition of magnetotelluric impedance tensor in the presence of local three-dimensional galvanic distortion. *J Geophys Res* 94:1913–1925. <https://doi.org/10.1029/JB094iB02p01913>
- Groom RW, Bailey RC (1991) Analytic investigations of the effects of near-surface three-dimensional galvanic scatterers on MT tensor decompositions. *Geophysics* 56(4):496–518
- Haak V (1980) Relations between electrical conductivity and petrological parameters of the crust and upper mantle. *Geophys Surv* 4:57–69. <https://doi.org/10.1007/BF01452958>
- Hansen C (1992) Analysis of discrete ill-posed problems by means of the L-curve. *SIAM Rev* 34:561–580. <https://doi.org/10.1137/1034115>

- Jödicke H (1992) Water and graphite in the earth's crust: an approach to interpretation of conductivity models. *Surv Geophys* 13:381–407. <https://doi.org/10.1007/BF01903484>
- Jones AG (1999) Imaging the continental upper mantle using electromagnetic methods. *Lithos* 48:57–80. [https://doi.org/10.1016/S0024-4937\(99\)00022-5](https://doi.org/10.1016/S0024-4937(99)00022-5)
- Jones AG (2013) Imaging and observing the electrical Moho. *Tectonophysics* 609:423–436. <https://doi.org/10.1016/j.tecto.2013.02.025>
- Jones AG, Ferguson IJ (2001) The electric Moho. *Nature* 409:331–333. <https://doi.org/10.1038/35053053>
- Jones AG, Jödicke H (1984) Magnetotelluric transfer function estimation improvement by a coherence-based rejection technique. In: Proceedings, 54th annual international society of exploration geophysicists meeting, Atlanta, Georgia, pp 51–55
- Jones AG, Kurtz RD, Boerner DE, Craven JA, McNeice GW, Gough DI, DeLaurier JM, Ellis RG (1992) Electromagnetic constraints on strikeslip fault geometry: the Fraser River fault system. *Geology* 20:561–564. [https://doi.org/10.1130/0091-7613\(1992\)020%3c0561:ecossf%3e2.3.co;2](https://doi.org/10.1130/0091-7613(1992)020%3c0561:ecossf%3e2.3.co;2)
- Kourim F, Bodinier J-L, Alard O, Bendaoud A, Vauchez A, Dautria J-M (2014) Nature and evolution of the lithospheric mantle beneath the Hoggar swell (Algeria): a record from mantle Xenoliths. *J Petrol* 55(11):2249–2280. <https://doi.org/10.1093/petrology/egu056>
- Krieger L, Peacock JR (2014) MTpy: a Python toolbox for magnetotellurics. *Comput Geosci* 72:167–175
- Lastoviskova M (1983) Laboratory measurement of electrical properties of rocks and minerals. *Geophys Surv* 6:201–213. <https://doi.org/10.1007/BF01454001>
- Lesquer A, Bourmatte A, Dautria JM (1988) Deep structure of the Hoggar domal uplift (Central Sahara, South Algeria) from gravity, thermal and petrological data. *Tectonophysics* 152:71–87. [https://doi.org/10.1016/0040-1951\(88\)90030-3](https://doi.org/10.1016/0040-1951(88)90030-3)
- Lesquer A, Bourmatte A, Ly S, Dautria JM (1989) First heat flow determination from the Central Sahara: relationship with the Pan-African belt and Hoggar domal uplift. *J Afr Earth Sci* 9:41–48. [https://doi.org/10.1016/0899-5362\(89\)90006-7](https://doi.org/10.1016/0899-5362(89)90006-7)
- Liégeois JP, Latouche L, Boughrara M, Navez J, Guiraud M (2003) The LATEA metacraton (Central Hoggar, Tuareg shield, Algeria): behaviour of an old passive margin during the Pan-African orogeny. *J Afr Earth Sci* 37:161–190. <https://doi.org/10.1016/j.jafears.2003.05.004>
- Liégeois J-P, Benhallou A, Azzouni-Sekkal A, Yahiaoui R, Bonin B (2005) The Hoggar swell and volcanism: reactivation of the Precambrian Tuareg shield during Alpine convergence and West African Cenozoic volcanism. In: Foulger GR, Natland JH, Presnall DC, Anderson DL (eds) Plates, plumes, and paradigms. Geological Society of America Special Paper 388, pp 379–400. <https://doi.org/10.1130/0-8137-2388-4.379>
- Liégeois J-P, Abdelsalam MG, Ennih N, Ouabadi A (2013) Metacraton: nature, genesis and behavior. *Gondwana Res* 23:220–237. <https://doi.org/10.1016/j.gr.2012.02.016>
- Liu HL, Gao SS (2010) Spatial variations of crustal characteristics beneath the Hoggar swell, Algeria, revealed by systematic analyses of receiver functions from a single seismic station. *Geochim Geophys Geosyst* 11:Q08011. <https://doi.org/10.1029/2010GC003091>
- Mackie R, Rieven S, Rodi W (1997) User's manual and software documentation for two-dimensional inversion of magnetotelluric data. Earth Resources Laboratory Rpt. Massachusetts Institute of Technology, Cambridge, p 13
- Marti A, Queralt P, Jones AG, Ledo J (2005) Improving Bahr's invariant parameters using the WAL approach. *Geophys J Int* 163:38–41. <https://doi.org/10.1111/j.1365-246X.2005.02748.x>
- Meqbel NM, Egberta GD, Wannamaker PhE, Kelbert A, Schultz A (2014) Deep electrical resistivity structure of the northwestern U.S. derived from 3-D inversion of USArray magnetotelluric data. *Earth Planet Sci Lett* 402:290–304. <https://doi.org/10.1016/j.epsl.2013.12.026>
- Nover G (2005) Electrical proprieties of crustal and mantle rocks: a review of laboratory measurements and their explanation. *Surv Geophys* 26:593–651. <https://doi.org/10.1007/s10712-005-1759-6>

- Parkinson WD (1962) The influence of continents and oceans on geomagnetic variations. *Geophys J Roy Astron Soc* 6:441–449. <https://doi.org/10.1111/j.1365-246X.1962.tb02992.x>
- Pasyanos ME, Walter WR (2002) Crust and upper-mantle structure of North Africa, Europe and the Middle East from inversion of surface waves. *Geophys J Int* 149:463–481. <https://doi.org/10.1046/j.1365-246X.2002.01663.x>
- Pérez-Gussinyé M, Metois M, Fernández M, Vergés J, Fullea J, Lowry AR (2009) Effective elastic thickness of Africa and its relationship to other proxies for lithospheric structure and surface tectonics. *Earth Planet Sci Lett* 287(1–2):152–167
- Priestley K, McKenzie D, Debayle E, Pilidou S (2008) The African upper mantle and its relationship to tectonics and surface geology. *Geophys J Int* 175:1108–1126
- Rao CK, Jones GA, Moorkamp M (2007) The geometry of the Iapetus Suture zone in central Ireland deduced from a magnetotelluric study. *Phys Earth Planet Inter* 161:134–141. <https://doi.org/10.1016/j.pepi.2007.01.008>
- Rao CK, Jones GA, Moorkamp M, Weckmann U (2014) Implications for the lithospheric geometry of the Iapetus suture beneath Ireland based on electrical resistivity models from deep-probing magnetotellurics. *Geophys J Int* 198(2):737–759. <https://doi.org/10.1093/gji/ggu136>
- Ritter O, Weckmann U, Vietor T, Haak V (2003) A magnetotelluric study of the Damara Belt in Namibia: 1. Regional scale conductivity anomalies. *Phys Earth Planet Inter* 138:71–90. [https://doi.org/10.1016/S0031-9201\(03\)00078-5](https://doi.org/10.1016/S0031-9201(03)00078-5)
- Roberts GG, White N (2010) Estimating uplift rate histories from river profiles using African examples. *J Geophys Res* 115:B02406. <https://doi.org/10.1029/2009JB006692>
- Rougier S, Missenard Y, Gautheron C, Barbarand J, Zeyen H, Pinna R, Liégeois J-P, Bonin B, Ouabadi A, Derder ME-M, Frison de Lamotte D (2013) Eocene exhumation of the Tuareg Shield (Sahara Desert, Africa). *Geology* 41:615–618. <https://doi.org/10.1130/G33731.1>
- Sebaï A, Stutzmann E, Montagner J-P, Sicilia D, Beuclerc E (2006) Anisotropic structure of the African upper mantle from Rayleigh and Love wave tomography. *Phys Earth Planet Inter* 155:48–62. <https://doi.org/10.1016/j.pepi.2005.09.009>
- Shankland TL, Ander M (1983) Electrical conductivity, temperatures and fluids in the lower crust. *J Geophys Res* 88:9475–9484. <https://doi.org/10.1029/JB088iB11p09475>
- Swift CM Jr. (1967) A magnetotelluric investigation of an electrical conductivity anomaly in the southwestern United States. Ph.D. thesis. Massachusetts Institute of Technology, Cambridge, p 223
- Takherist D, Lesquer A (1989) Mise en évidence d'importantes variations régionales du flux de chaleur en Algérie. *Can J Earth Sci* 26(4):615–626. <https://doi.org/10.1139/e89-053>
- Tikhonov AN (1950) Determination of electrical characteristics of the deep strata of the earth's crust. *Dokl Akad Nauk SSSR* 73:292–297
- Unsworth M, Bedrosian PA (2004) On the geoelectric structure of major strike-slip faults and shear zones. *Earth Planet Space* 56:1177–1184
- Wannamaker PhE, Hasterok DP, Johnston JM, Stodt JA, Hall DB, Sodergren TL, Pellerin L, Maris V, Doerner WM, Groenewold KA, Unsworth MJ (2008) Lithospheric dismemberment and magmatic processes of the Great Basin–Colorado Plateau transition, Utah, implied from magnetotellurics. *Geochem Geophys Geosyst* 9:Q05019. <https://doi.org/10.1029/2007GC001886>
- Zerrouk S, Bendaoud A, Hamoudi M, Liégeois J-P, Boubekri H, Ben El Khaznadj R (2016) Mapping and discriminating the Pan-African granitoids in the Hoggar (southern Algeria) using Landsat 7 ETM+ data and airborne geophysics. *J African Earth Sci* 127:146–158. <https://doi.org/10.1016/j.jafrearsci.2016.10.003>